Zhang Yan-Lin (Orcid ID: 0000-0002-8722-8635)

Lin Yu-Chi (Orcid ID: 0000-0003-4227-8978)

Zhao Zhu-Yu (Orcid ID: 0000-0002-6465-931X)

Sun Yele (Orcid ID: 0000-0003-2354-0221)

Qiu Yanmei (Orcid ID: 0000-0002-0912-2675)

Wang Yuxuan (Orcid ID: 0000-0002-1649-6974)

Changes of Emission Sources to Nitrate Aerosols in Beijing after the Clean Air Actions: Evidence from Dual Isotope Compositions

Mei-Yi Fan[1,2,3], Yan-Lin Zhang[1,2,3]*, Yu-Chi Lin[1,2,3], Fang Cao[1,2,3], Zhu-Yu Zhao[1,2,3], Yele Sun[4,5,6], Yanmei Qiu[4,5], Pingqing Fu[7], Yuxuan Wang[8,9]

[1.] Yale-NUIST Center on Atmospheric Environment, International Joint Laboratory on Climate and Environment Change, Nanjing University of Information Science and Technology, Nanjing, 210044, China

[2.] Key Laboratory Meteorological Disaster; Ministry of Education & Collaborative Innovation Center on Forecast and Evaluation of Meteorological Disaster, Nanjing University of Information Science and Technology, Nanjing, 210044, China

[3.] Jiangsu Provincial Key Laboratory of Agricultural Meteorology, College of Applied Meteorology, Nanjing University of Information Science & Technology, Nanjing 210044, China

[4.] State Key Laboratory of Atmospheric Boundary Layer Physics and Atmospheric Chemistry,

This article has been accepted for publication and undergone full peer review but has not been through the copyediting, typesetting, pagination and proofreading process which may lead to differences between this version and the Version of Record. Please cite this article as doi: 10.1029/2019JD031998

Institute of Atmospheric Physics, Chinese Academy of Sciences, Beijing 100029, China

[5.] *University of Chinese Academy of Sciences, Beijing 100049, China*

[6.] *Center for Excellence in Regional Atmospheric Environment, Institute of Urban Environment, Chinese Academy of Sciences, Xiamen 361021, China*

[7.] *Institute of Surface-Earth System Science, Tianjin University, Tianjin, 300072, China*

[8.] *Department of Earth and Atmospheric Sciences, University of Houston, Houston, TX, 77204, United States*

[9.] *Institute for Climate and Atmospheric Science, University of Houston, Houston, TX, 77204, United States*

*Corresponded to Yan-Lin Zhang (*zhangyanlin@nuist.edu.cn ; dryanlinzhang@outlook.com*)*

Key points:

1. Nitrate aerosols in Beijing during the haze events were mainly produced by hydrolysis of N_2O_5 under high humidity conditions.
2. The contribution of coal combustion to atmospheric nitrate decreased significantly after clean air actions implemented by Chinese government.
3. Strict control of traffic emissions would be an important way to decrease nitrate concentrations and improve the air quality in Beijing.

ABSTRACT

Nitrate (NO_3^-) is a major contributing species to haze formation in Northern China. So far, formation processes and source apportionments of nitrate aerosols during haze pollution have not yet been well understood. In this study, the $PM_{2.5}$ samples were collected in Beijing from November 13 to December 24, 2018. In addition to water-soluble ions, oxygen ($\delta^{18}O\text{-}NO_3^-$) and nitrogen ($\delta^{15}N\text{-}NO_3^-$) isotopes in particulate NO_3^- were also determined, in order to investigate the formation pathways and potential sources of NO_3^- aerosols. The results showed that NO_3^- was a dominant species (43%) of secondary inorganic aerosols during the sampling period. The $\delta^{18}O\text{-}NO_3^-$ and $\delta^{15}N\text{-}NO_3^-$ values averaged at 83.8±13.4 and 11.5±5.0‰, respectively. Combining isotope compositions and Bayesian isotope mixing model, we found that heterogeneous reaction and gas-phase oxidation contributed equally to nitrate formation during the sampling period. However, the contribution of heterogeneous processes to nitrate increased from 39% during the clean period to 64% during the haze period. On average, coal combustion, biomass burning, vehicle emissions and soil emission contributed 50, 26, 20 and 4%, respectively, to nitrate aerosols during the sampling period. Compared to the result in 2013, the significant decrease (~21%) of relative contribution of coal combustion to nitrate was due to strict reduction of coal consumption in Beijing. Finally, the relative contribution of traffic emissions to nitrate increased from 18% during the clean period to 30% during the haze period, suggesting that control of traffic emissions would be an important way to decrease nitrate concentrations and improve the air quality in Beijing.

Keywords: Nitrate aerosols, Haze events, Stable isotopes, Formation mechanism, Source apportionment

1. Introduction

Fine particulate matter (aerodynamic diameter smaller than 2.5 μm, $PM_{2.5}$) pollution is a serious environmental problem worldwide and has adverse effects on human health and ecosystem [*Clark and Tilman*, 2008; *Zhang et al.*, 2017]. Nitrate (NO_3^-), a key species of $PM_{2.5}$, is a major contributing species to haze events in China due to enhancements of its absolute concentration and relative contribution to $PM_{2.5}$ mass [*Fan et al.*, 2019; *Pan et al.*, 2016]. Formation of atmospheric nitrate is mainly influenced by its precursor concentrations (NO_x = NO_2 + NO) and meteorological factors. For example, lower temperature (T), higher relative humidity (RH) and low wind speed are favorable conditions for the formation and accumulation of nitrate aerosols in the atmosphere. Nitrate is mainly produced from its precursor NO_x, which is emitted from industries, vehicle exhausts, biomass burning (BB, including burning of crop residues and residential heating) and agricultural soils; therefore quantification of potential sources of NO_x will give us a hint to understand the potential sources of particulate nitrate and help policy-makers to formulate strategies to reduce nitrate concentrations and decrease the haze formation in China.

Chemical transformation of NO_x to nitrate includes gas-phase oxidation and heterogeneous process. In gas-phase oxidation, NO is emitted into the atmosphere and then immediately oxidized by O_3 or HO_2/RO_2 to produce NO_2. Subsequently, NO_2 reacts with hydroxyl radicals ($OH^{\cdot}$) to yield nitric acid (HNO_3) and then transforms to nitrate aerosols by reacting with NH_3. Previously, gas-phase oxidation process was regarded as a dominant pathway of nitrate formation at daytime [*Khoder*, 2002]. On the contrary, hydrolysis of nitrogen pentoxide (N_2O_5) in the preexisting aerosols is considered a major mechanism for nitrate formation, especially during nighttime. This mechanism has been proved to be a pivotal pathway of nitrate production during the Chinese haze events [*Li et al.*, 2018; *Wang et al.*, 2017].

To date, sources of secondary related aerosols such as NO_3^- are very difficult to identify; however, isotope technique is a useful tool to explore potential sources and formation mechanisms of particulate nitrate [*Alexander et al.*, 2009; *Chang et al.*, 2018; *Kamezaki et al.*, 2019; *Song et al.*, 2019; *Zong et al.*, 2017]. Nitrogen isotope of NO_3^- ($\delta^{15}N\text{-}NO_3^-$) can be used to identify the sources of atmospheric nitrate by comparing with $\delta^{15}N$ of NO_x in certain emission sources [*Chang et al.*, 2018; *Kendall et al.*, 2007; *Morin et al.*, 2008; *Song et al.*,

2019]. The isotope fractionation of 7.8 to 11.0 ‰ from NO_x to NO_3^- has to be considered when using isotope techniques to track sources of particulate nitrate [*Chang et al.*, 2018; *Fan et al.*, 2019; *Song et al.*, 2019]. Previous studies have shown that the difference between $\delta^{15}N$ of $NO_{2\,(g)}$ and oxidized $HNO_{3\,(g)}$ was about -3 ‰ due to the kinetic reaction, and was much lower than isotope equilibrium fractionations occurred in the photochemical cycle between NO and NO_2 (34 ‰) [*Freyer*, 1991]. *Zong et al.* [2017] proposed an approach to calculate the isotope fractionation coefficients by combining $\delta^{15}N\text{-}NO_3^-$ values with the Bayesian mixing model. Considering the effects of isotope fractionation, *Zong et al.* [2017] pointed out that coal combustion was the predominant source of $PM_{2.5}$ nitrate (~ 60 %) at Beihuangchen Island, a regional background site in northern China, during the wintertime. The oxygen isotope fractionation during the transformation of NO_x to NO_3^- involves two oxidation processes: one is NO_2 + OH and another one is $N_2O_5 + H_2O$ [*Hastings et al.*, 2003; *Wankel et al*., 2010]. Due to the different consumption of O atom in the two pathways, oxygen isotopes compositions ($\delta^{18}O$ and $\Delta^{17}O$) in nitrate would be distinctive and therefore oxygen isotope has been used for differentiating the formation mechanisms of airborne nitrate aerosols recently [*Song et al*., 2019; *Wang et al*., 2019].

Nitrate in $PM_{2.5}$ is mainly attributed to secondary transformation from NO_x. Coal combustion contributed a major fraction (~ 50 %) to atmospheric NO_x in Hebei-Beijing-Tianjin area based on the emission inventories in 2003 [*Zhao et al*., 2012]. This suggested that coal burning might be a major source of nitrate aerosols in Beijing. However, coal consumption in Beijing has been strictly reduced and some strategies of control in NO_x emissions has also been conducted through clean air actions since 2013. Due to the changes of NO_x emission in recent years, the changes of source apportionments of particulate nitrate would be expected. Thus, tracking potential sources of particulate nitrate after the alteration of NO_x emissions is needed. In this study, the ambient $PM_{2.5}$ samples were collected in Beijing during November 13 to December 24, 2018. In addition to water-soluble ions, $\delta^{15}N\text{-}NO_3^-$ and $\delta^{18}O\text{-}NO_3^-$ values were also determined. The relative contributions of gas-phase oxidation (NO_2 + OH) and heterogeneous process ($N_2O_5 + H_2O$) to NO_3^- aerosol formation were quantified by isotope compositions combining with the Bayesian model. After considering isotope fractionation effect between NO_x and NO_3^-, the emission sources of particulate nitrate in Beijing were

quantified. Limited to our knowledge, this is the first time to identify the potential sources of particulate nitrate in Beijing after the strict reduction of coal consumption. Thus, the results were also compared with the earlier study to understand the evolution of dominant sources to nitrate aerosols in Beijing before and after the clean air actions.

2. Methodology

2.1 Sampling

$PM_{2.5}$ samples were collected on the campus of the Institute of Atmospheric Physics, the Chinese Academy of Sciences (IAPCAS, 39º 58' N, 116 º 22' E), located in Beijing, China from 13 November to 24 December, 2018. The sampling site is surrounded by residential areas and major roads without industrial emission sources nearby. During the sampling period, the aerosol sampler was installed at a height of 14 m above the ground, on the rooftop of a three-story building. Each aerosol sample was collected from 8:30 (local time, LT) to 18:30 LT and from 18:30 LT to 8:30 LT on the next day. A high-volume sampler (Tisch-$PM_{2.5}$, USA, flow rate was approximately 1.1 m^3 min^{-1}) was employed to collect $PM_{2.5}$ samples and quartzes filters (TISSUQUARTZ-2500QAT-UP, size: 8 × 10 in, PALL USA) were used as filtration filters. Prior to sampling, the filters were heated in an oven at 450 °C for 6 h to remove impurities from the filters. After sampling, each filter was folded and stored in a separate plastic that was then stored in a polypropylene container, frozen immediately, and returned to the laboratory for further chemical analyses. During the sampling period, the concentrations of $PM_{2.5}$ mass and trace gases (CO, NO_2) were obtained from the Beijing Air Quality Monitoring Station (approximately 2.1 km distance from the sampling site). Moreover, the meteorological data, including ambient T and RH (HC2-S3, Rotronic, Switzerland), wind speed (WS) and wind direction (WD) (010C cup anemometers and 020C wind vanes, Metone, USA) were obtained from the Beijing meteorological tower at an altitude of 32 m, which is also situated on the campus of IAPCAS.

2.2 Chemical and isotopic analysis

After sampling, the concentrations of inorganic ions (NO_3^-, SO_4^{2-}, Cl^-, NH_4^+, K^+, Na^+,

Ca^{2+}) were measured by an ion chromatograph (ICS 5000+, Thermo Scientific, USA). One piece of the sampled filter with an area of 2.54 cm^2 was punched and put into a Teflon vessel. Subsequently, the sampled filter was extracted with 15 mL Milli-Q water (18.2 Ω) for 30 minutes. The details of accessories (suppressor, chromatographic column, etc.) of the ion chromatography as well as detection limits (DLs) and uncertainty of ions through this method can be found in the previous work [*Fan et al.*, 2019]. Nitrate is the targeted species in this study; the DL and uncertainty of NO_3^- were 0.08 ng m^{-3} and 2 %, respectively.

N and O isotope analysis was based on the isotopic analysis of dinitrogen oxide (N_2O) after chemical conversion of NO_3^- to N_2O [*Zhao et al.*, 2019]. Briefly, a small piece of the sampled filter (containing at least 1 μg N) was extracted with 5 ml Milli-Q water for 30 minutes. After extraction, the solution was then filtered by a membrane filter (0.22 μm) and prepared to proceed chemical conversion procedure. In the conversion process, NO_3^- was initially transformed to NO_2^- by cadmium (Guaranteed reagent GR, Alfa Aesar, US). Subsequently, NO_2^- was reduced to N_2O by sodium azide (NaN_3) in an acetic acid buffer. The produced N_2O was then analyzed N and O isotope by an isotope ratio mass spectrometer (MAT253, Thermo Fisher Scientific, US) couple with a multi-purpose online gas preparation device (GasBench) and trace gas preconcentration device (Precon, at 21°C) at ion source voltage of 9.50 KV and with a high purity of xenon (99.999 %, Liquid Gas, Shanghai), which was used as a carrier gas. The QA/QC was guaranteed by analyzing the international NO_3^- standard (IAEA-NO-3: $\delta^{18}O_{SMOW}$ = 25.6 ‰, $\delta^{15}N_{Air}$ = 4.7 ‰ and USGS35: $\delta^{18}O_{SMOW}$ = 57.5 ‰, $\delta^{15}N_{Air}$ = 2.7 ‰) in the same procedure as real samples. The measured values of IAEA-NO-3 and USGS35 were 25.09 ± 0.34 ‰ and 56.90 ± 0.13 ‰ for $\delta^{18}O$ and 4.88 ± 0.07 ‰ and 2.74 ± 0.09 ‰ for $\delta^{15}N$, respectively, suggesting that this method can be used to accurately measure N and O isotopes in NO_3^- in atmospheric aerosol samples. Finally, the ^{15}N and ^{18}O isotope values of N_2O were analyzed and reported in parts per thousand relative to standards (USGS32: $\delta^{15}N$ = + 180 ‰, $\delta^{18}O$ = + 25.7 ‰; USGS34: $\delta^{15}N$ = - 1.8 ‰, $\delta^{18}O$ = - 27.9 ‰) [*Böhlke et al.*, 2003]:

$$\delta^{15}N = [(^{15}N/^{14}N)_{sample}/(^{15}N/^{14}N)_{standard} - 1] \times 1000 \quad (1)$$

$$\delta^{18}O = [(^{18}O/^{16}O)_{sample}/(^{18}O/^{16}O)_{standard} - 1] \times 1000 \quad (2)$$

The $\delta^{15}N$ and $\delta^{18}O$ differences in standards and samples repetitions were less than 0.08 ‰ and 0.24 ‰ to ensure the analytical precision. The details of this method can be found in elsewhere

[*Zhao et al*., 2019]

2.3 Bayesian isotope mixing model

A Bayesian isotope mixing model run in the R software package (Stable Isotope Analysis in R, SIAR) was used to calculate fractionation coefficient between NO_x and NO_3^- and estimate the formation processes and potential sources of atmospheric nitrate aerosols. Details of SIAR can be found elsewhere [*Parnell et al.*, 2010]. Briefly, a logical prior distribution was established firstly in this model and then the probability distribution of the contribution of each source to the mixture was determined [*Parnell et al.*, 2010]. To achieve the purpose of the SIAR model, a set of N mixture measurements on j isotopes with k source contributors are defined as follows:

$$\mathrm{X}_{ij} = \sum_{k=1}^{k} P_k(S_{jk} + C_{jk}) + \varepsilon_{ij}$$

$$S_{jk} \sim N(\mu_{jk}, \omega_{jk}^2)$$

$$C_{jk} \sim N(\lambda_{jk}, \tau_{jk}^2)$$

$$\varepsilon_{ij} \sim N(0, \sigma_j^2) \qquad (3)$$

Where P_k represents the proportion of source k identified by the SIAR model and all P_k values sum to 1 (unity); X_{ij} is the isotope value j of the mixture i, in which i = 1, 2, ..., N and j = 1, 2, ..., J; S_{jk} is the source value k (k = 1, 2, …, K) on isotope j and is distributed with mean value (μ_{jk}) and standard deviation (ω_{jk}), which is related with the source values in Table S1; C_{jk} represents the trophic enrichment factor for isotope j on source k which is distributed with mean (λ_{jk}=0) and standard deviation (τ_{jk}=1); in addition ε_{ij} is the residual error represented the additional unquantified variation between individual mixtures which is distributed with mean 0 and standard deviation (σ_j=1).

2.4 Backward trajectory analysis

To realize the influence of origins and transported routes of air parcels on isotope compositions and potential sources of particulate nitrate measured in Beijing, the back-trajectories were computed by the Hybrid Single-particle Lagrangian Integrated Trajectory

(HYSPLIT) model (http://www.arl.noaa.gov/ready/hysplit4.html) developed by US NOAA Air Resources Laboratory [*Draxler and Hess*, 1998]. The meteorological data for creating the trajectories was the GDAS (Global Data Assimilation System) (ftp://arlftp.arlhq.noaa.gov/pub/archives/gdas1/), which were processed by the NCEP with a 6-hour time resolution, about 190 km horizontal resolution and 23 vertical levels. In this work, 24-hour backward trajectories arriving at 100 m were computed at 8:00 LT and 18:00 LT with a time step of 6 hours for the daytime and nighttime samples, respectively. During the sampling periods, a total of 83 trajectories were obtained. The classifications of transported routes of the air parcels and their influences on particulate nitrate sources will be discussed in the following section.

3. Results and discussion

3.1 Overview of $PM_{2.5}$ and water-soluble ions

Figure 1 shows the time series of concentrations of $PM_{2.5}$ mass, water-soluble ions, trace gases and meteorological parameters at the receptor sites during the sampling period. The results showed that $PM_{2.5}$ mass concentrations varied from 4.3 to 289.6 μg m^{-3} with a mean value of 69.3 ± 68.9 μg m^{-3} (see in Table 1). The average concentration of total water-soluble inorganic ions (TWSIIs) was 26.7 ± 34.6 μg m^{-3}, which accounted for 40 % of $PM_{2.5}$ mass. NO_3^-, NH_4^+ and SO_4^{2-} were the dominant ionic species, accounting for 17, 9 and 7 % of $PM_{2.5}$ mass, respectively. The rest of other components in $PM_{2.5}$ were organic materials and elemental carbon along with trace elements [*Zhang et al.*, 2015]. The concentrations of $PM_{2.5}$ mass and ions in the daytime and nighttime samples are also listed in Table 1. As can be seen, the average concentration of $PM_{2.5}$ mass of the nighttime samples was 73.4 ± 64.6 μg m^{-3}, which was slightly higher than that (65.2 ± 73.5 μg m^{-3}) of the daytime samples. The higher $PM_{2.5}$ concentration of the nighttime samples might be associated with lower boundary layer in the dark, which was favorable for accumulation of air pollutants [*Du et al.*, 2013]. However, no significant differences of the concentrations in terms of water-soluble inorganic ions were observed between the daytime and nighttime samples.

The ion balance between anions and cations is shown in Figure S1. In this figure, the

equivalent concentrations (μeq m^{-3}) of cations (C) and anions (A) can be calculated as:

$$C=\frac{Na^+}{23}+\frac{NH_4^+}{18}+\frac{K^+}{39}+\frac{2\times Mg^{2+}}{24}+\frac{2\times Ca^{2+}}{40} \quad (4)$$

$$A=\frac{2\times SO_4^{2-}}{96}+\frac{NO_3^-}{62}+\frac{Cl^-}{35.5}+\frac{2\times C_2O_4^{2-}}{88} \quad (5)$$

A good correlation coefficient (r = 0.99, significance at 95% confidence interval, $p < 0.05$) between cation and anion equivalent concentrations was found with a slope of 1.1. The equivalent concentrations of anions were slight lower than those of cations. This might be attributed to the organic ions which were not measured in these samples. This is true since organic ions, predominated by organic acids, accounted for 3.7 % in TWSIIs in Beijing [*Huang et al*., 2005]. A high correlation between cation and anion with a ratio of cation-to-anion approaching to 1.0 suggested that our data exhibited good quality and was able to be used for further analysis of scientific issues.

To study the evolutions of ions in the different $PM_{2.5}$ levels, we further divided the aerosol samples into three categories, namely, clean ($PM_{2.5} \leq 75$ μg m^{-3}), moderate (75 μg $m^{-3} < PM_{2.5} \leq 150$ μg m^{-3}) and haze conditions ($PM_{2.5} > 150$ μg m^{-3}). Figure 2a shows the concentrations of water-soluble ions in the different pollution levels. The TWSIIs mass concentrations during the clean and haze periods were 11.4 and 100.2 μg m^{-3}, respectively. The ratio of TWSIIs/$PM_{2.5}$ mass rose from 32 % on the clean days to 50 % on the severe haze days, indicating that dramatic enhancements of TWSIIs were observed during the haze events.

Apparent increases of absolute concentrations of all ions were found when the $PM_{2.5}$ concentrations increased. When we checked the relative contribution of each ion to $PM_{2.5}$ mass under the different $PM_{2.5}$ levels, some interesting results were found (Figure 2b). The relative contributions of nitrate to TWSIIs were 38, 45 and 46 % during the clean, moderate and severe polluted conditions. In contrast, the relative abundances of sulfate and ammonium kept almost constant levels under different $PM_{2.5}$ regimes. The contributions of other ions, including K^+, Ca^{2+} and Cl^-, to $PM_{2.5}$ mass kept constant levels or decreased during the severe pollution conditions. These findings elucidated that nitrate was a major contributing species to $PM_{2.5}$ during the severe haze period in Beijing.

In the current work, the mass ratio of NO_3^-/SO_4^{2-} averaged at 1.9 ± 1.1 (see in Table 1). This value was much higher than those in Xi'an (0.9), Guangzhou (0.6) and Beijing (0.8) of

the previous studies [*Huang et al.*, 2014; *Liu et al.*, 2014; *Zhang et al.*, 2011]. Indeed, the high nitrate-to-sulfate mass ratio of > 1 was also observed in other mega-cities over China in recent years [*Yu et al.*, 2019; *Zhang et al.*, 2019; *Zhang et al.*, 2018]. To improve air quality, the Chinese government has reduced its anthropogenic emissions by 62 % for SO_2 and 17 % for NO_x from 2010 to 2017 [*Zheng et al*., 2018]. The reduction rate of SO_2 was evidently higher than that of NO_x. This might give a reasonable explanation for enhanced NO_3^-/SO_4^{2-} ratio in ambient PM in recent years.

3.2 Isotopic values of $^{15}N\text{-}NO_3^-$ and $^{18}O\text{-}NO_3^-$ in $PM_{2.5}$

Figure 3 shows the time series of NO_3^- concentrations, $\delta^{15}N\text{-}NO_3^-$ and $\delta^{18}O\text{-}NO_3^-$values during the sampling period. The $\delta^{15}N\text{-}NO_3^-$ values varied from -0.8 to 20.6 ‰ with a mean value of 11.4 ± 5.0 ‰. This value was comparable to those in Beijing (11.9 ± 4.4 ‰ in 2014 winter) [*Song et al.,* 2019] and Seoul in the 2015 and 2016 wintertime (11.9 ± 2.5 ‰) [*Park et al.*, 2018], but was much higher than those in coastal Antarctica (-17.9 to -32.7 ‰) [*Savarino et al.*, 2007], the Midwestern and the Northeastern United States (+3.2 to -8.1 ‰) [*Elliott et al.*, 2007]. This might indicate that nitrate in Beijing and Seoul was mianly affected by the emission sources containing enriched $\delta^{15}N$ value such as coal combustion (13.7 ± 4.6 ‰) [*Felix et al*., 2015; *Felix et al*., 2012 ; *Walter et al*., 2015a], whereas the nitrate aerosols in the United States and coastal Antarctica were mainly contributed by the sources which possessed depleted $\delta^{15}N$ value such as vehicle exhausts (-3.2 ± 6.8 ‰) [*Walter et al*., 2015b] or soil emission (-33.77 ± 12.16 ‰) [*Felix and Elliott*, 2014; *Li and Wang*, 2008]. The average $\delta^{15}N\text{-}NO_3^-$ value of the daytime samples (12.4 ± 5.1 ‰) was similar to that of the nighttime samples (10.4 ± 4.7 ‰). Figure 4a plots the $\delta^{15}N\text{-}NO_3^-$ values under various $PM_{2.5}$ levels. The average $\delta^{15}N\text{-}NO_3^-$ values during the clean and moderate polluted conditions were 12.0 ‰ and 13.4 ‰, respectively. When $PM_{2.5}$ exceeded 150 μg m^{-3}, the $\delta^{15}N\text{-}NO_3^-$ decreased abruptly to 6.0 ‰. The depleted $\delta^{15}N\text{-}NO_3^-$ value indicated that particulate NO_3^- was from different sources during the severe polluted events and this will be discussed in the following section.

The $\delta^{18}O\text{-}NO_3^-$ values in $PM_{2.5}$ during the 2018 winter varied from 50.3 to 106.6 ‰ with a mean value of 83.4 ± 13.9 ‰. The mean $\delta^{18}O\text{-}NO_3^-$ values of the daytime and nighttime samples were 85.6 ± 10.2 ‰ and 81.1 ± 16.6 ‰, respectively, showing no difference of $\delta^{18}O$-

NO_3^- value between the daytime and nighttime aerosol samples. Such similar isotope composition in the daytime and nighttime samples might be interpreted by two reasons. The short-time resolution sampling (e.g. 10 h /14 h in this study) could not distinguish completely daytime aerosols from nighttime ones [*He et al*., 2020; *Sun et al*., 2018]. Another reason might be due to the long residence time of atmospheric particulate nitrate, which was usually longer than 12 hours in the troposphere and its diurnal variation was difficult to captured [*Vicars et al*., 2013]. Here, we recommended to develop a technique for high-time resolution measurements of isotope compositions (e.g. $\delta^{15}N\text{-}NO_3^-$ and $\delta^{18}O\text{-}NO_3^-$) and this can be efficiently used to study the diel cycles of formation mechanisms and source apportionments of nitrate aerosols. Figure 4b shows $\delta^{18}O\text{-}NO_3^-$ values under different pollution conditions. The average $\delta^{18}O\text{-}NO_3^-$ value in the clean events was 79.6 ± 13.3 ‰, which was much lower than those during the moderate (96.7 ± 5.3 ‰) and haze (91.8 ± 9.8 ‰) conditions. The discrepancies of $\delta^{18}O\text{-}NO_3^-$ suggested that different relative contributions of NO_2 + OH and $N_2O_5 + H_2O$ to nitrate formation under different pollution conditions [*Wang et al.*, 2019]. Thus, the significant increased $\delta^{18}O\text{-}NO_3^-$ suggested that different formation pathways of nitrate aerosols under moderate and haze conditions and this will be discussed in the next section.

3.3 Relative contributions of nitrate formation pathways in $PM_{2.5}$

In this section, the relative contributions of NO_2+OH (f_{OH}) and $N_2O_5 + H_2O$ (f_{N2O5}) to particulate NO_3^- formation were estimated by using observed $\delta^{18}O\text{-}NO_3^-$ values combined with SIAR model. Assuming that airborne nitrate aerosols are mainly produced by NO_2 + OH ($[\delta^{18}O\text{-}NO_3^-]_{OH}$) and $N_2O_5 + H_2O$ ($[\delta^{18}O\text{-}NO_3^-]_{N2O5}$); subsequently, the $\delta^{18}O\text{-}NO_3^-$ can be calculated as [*Walters et al.*, 2016; *Zong et al.*, 2017]:

$$\delta^{18}O\text{-}NO_3^- = f_{N2O5} \times [\delta^{18}O\text{-}NO_3^-]_{N2O5} + f_{OH} \times [\delta^{18}O\text{-}NO_3^-]_{OH} \quad (6)$$

and $f_{N2O5} + f_{OH} = 1$.

In Eq. (6), $[\delta^{18}O\text{-}NO_3^-]_{N2O5}$ and $[\delta^{18}O\text{-}NO_3^-]_{OH}$ denote $\delta^{18}O$ in NO_3^- produced by $N_2O_5 + H_2O$ and NO_2 + OH processes, respectively. The $[\delta^{18}O\text{-}NO_3^-]_{N2O5}$ and $[\delta^{18}O\text{-}NO_3^-]_{OH}$ can be estimated by the Eqs. (7) and (8):

$$[\delta^{18}O\text{-}NO_3^-]_{N2O5} = 1/6 \times (\delta^{18}O\text{-}H_2O) + 5/6 \times (\delta^{18}O\text{-}N_2O_5) \quad (7)$$

$$[\delta^{18}O\text{-}NO_3^-]_{OH} = 1/3 \times [\delta^{18}O\text{-}OH]_{OH} + 2/3 \times [\delta^{18}O\text{-}NO_2]_{OH} \quad (8)$$

where $[\delta^{18}O\text{-}OH]_{OH}$ and $[\delta^{18}O\text{-}NO_2]_{OH}$ are the $\delta^{18}O$ values in the atmospheric OH· and NO_2. In Eq. (7), $(\delta^{18}O\text{-}H_2O)$ is $\delta^{18}O$ values in tropospheric water (-25 ‰ to 0 ‰) [*Dubey et al*., 1997] and $\delta^{18}O\text{-}N_2O_5$ is the $\delta^{18}O$ value in the N_2O_5 with the range from 90 ‰ to 122 ‰ [*Johnston and Thiemens*, 1997].

In Eq. (8), $[\delta^{18}O\text{-}OH]_{OH}$ and $[\delta^{18}O\text{-}NO_2]_{OH}$ can be obtained from Eq. (9) and (10):

$$[\delta^{18}O\text{-}OH]_{OH} = 1000 \times ({}^{18}\alpha_{OH/H2O} - 1) + (\delta^{18}O\text{-}H_2O) \quad (9)$$

$$[\delta^{18}O\text{-}NO_2]_{OH} = 1000 \times ({}^{18}\alpha_{NO2/NO} - 1)(1- f_{NO2})/[({}^{18}\alpha_{NO2/NO} \times f_{NO2}) + (1- f_{NO2})] + (\delta^{18}O\text{-}NO_x) \quad (10)$$

In Eq. (10), $\delta^{18}O\text{-}NO_x$ is the $\delta^{18}O$ values in atmospheric NO_x, which range from 90 – 122 ‰. f_{NO2} is the mass fraction of NO_2 to NO_x. Nevertheless, NO_2 and NO_x concentrations were not observed in this work and therefore the ratio of NO_2 to NO_x was assumed to be in the range of 0.2-0.95, in order to obtain $[\delta^{18}O\text{-}NO_2]_{OH}$ values. [*Walters and Michalski*, 2016]. ${}^{18}\alpha_{OH/H2O}$ (${}^{18}\alpha_{NO2/NO}$) is the equilibrium isotope fractionation factor of $\delta^{18}O$ between OH· and H_2O (NO_2 to NO) and can be calculated by the following formula:

$${}^{18}\alpha_{X/Y} - 1 = 1/1000 \times [(A / T^4 \times 10^{10}) + (B / T^3 \times 10^8) + (C/T^2 \times 10^6) + (D/T \times 10^4)] \quad (11)$$

where A, B, C and D are the constants with the values of 2.1137, -3.8026, 2.2653 and 0.5941 for ${}^{18}\alpha_{OH/H2O}$ estimation, and -0.04129, 1.1605, -1.8829 and 0.74723 in terms of ${}^{18}\alpha_{NO2/NO}$ calculation [*Walters and Michalski*, 2016]. T is the ambient temperature (K).

Based on observed $\delta^{18}O\text{-}NO_3^-$ values of $PM_{2.5}$ and Eqs. (6 - 11), 10000 feasible solutions of f_{OH} were generated through the Monte Carlo simulation performed in the SIAR model. Then, the f_{N2O5} were calculated by 1- f_{OH}.

As mentioned above, we assumed that the ratio of NO_2 to NO_x was in a range of 0.2-0.95 for the estimations of nitrate formation pathways. Here, the sensitivity of NO_2/NO_x ratio to the contribution of gas-phase oxidation to nitrate formation was also tested. In this test, the NO_2/NO_x ratio was assumed to be 0.2, 0.5, 0.7, 0.9 and 0.95. Figure S2 shows the contributions of NO_2 + OH to nitrate aerosol formation depending on various NO_2/NO_x ratios. The contribution of NO_2 + OH to nitrate formation increased from 49 % to 53 % when the ratio of NO_2/NO_x ratio increased from 0.2 to 0.95. In other words, the contribution of heterogeneous process to nitrate production decreased from 51 % to 47 % when the NO_2/NO_x ratio increased from 0.2 to 0.95. This suggested that NO_2/NO_x ratio would not significantly influence the

estimated results. Consequently, the NO_2/NO_x ratio was assumed to be 0.2 to 0.95 for the following estimations.

Figure S3 plots the time series of relative contributions of $NO_2 + OH\cdot$ and $N_2O_5 + H_2O$ to particulate nitrate formation during the sampling period. On average, the f_{N2O5} and f_{OH} values were 48 ± 26 % and 52 ± 26 %, respectively. Some recent studies have pointed out that heterogeneous reaction is a major formation pathway of particulate nitrate formation. For instance, *Alexander et al.* [2009] estimated that 55 % of nitrate particles in northern China were formed by $N_2O_5 + H_2O$. *Wang et al.* [2019] suggested that the hydrolysis of N_2O_5 on aerosol surface produced approximately 69 % of ambient particulate nitrate in Beijing. In this work, the relative contribution of $NO_2 + OH\cdot$ was almost equal to that of $N_2O_5 + H_2O$ (52 % vs. 48 %), indicating that both gas-phase oxidation and heterogeneous processes played important roles in producing nitrate aerosols in Beijing during the sampling period. The relative contribution of NO_2 + OH and $N_2O_5 + H_2O$ to particulate nitrate depending on various $PM_{2.5}$ levels are shown in Figure 5. When $PM_{2.5}$ concentration was lower than 75 μg m^{-3}, the contribution of heterogeneous processes to nitrate production was nearly 39 ± 25 %. When the $PM_{2.5}$ concentration exceeded 150 μg m^{-3}, high particulate nitrate concentrations were mainly driven by the reaction of $N_2O_5 + H_2O$, accounting for 64 % of total nitrate aerosol production. The high contribution of heterogeneous process to nitrate formation might be expected during the polluted air since declined $OH\cdot$ concentrations were found due to weak photooxidation under haze conditions [*Bäumer et al.*, 2008] and resulted in lower contribution of homogeneous reaction to nitrate production. In Beijing, high nitrate concentrations via hydrolysis of N_2O_5 have been reported in the recent studies [*Wang et al*., 2018; *Yan et al*., 2019]. They concluded that the humid air accelerated nitrate aerosol production during haze pollution.

Figures 6(a) and (b) show the relative contributions of N_2O_5 pathway to nitrate under different RH and aerosol liquid water content (ALWC) conditions. In this figure, ALWC was calculated by ISSOROPIA II model (see supplementary S1, *Fountoukis and Nenes*, 2007), which has been widely employed to estimate ALWC in many studies [*Deng et al.*, 2016; *Fan et al.*, 2019; *Tan et al.*, 2017]. As can be seen, the relative contributions of heterogeneous processes to nitrate production increased obviously with increases of relative humidity and ALWC. On the other hand, the fractions of heterogeneous reaction to nitrate formation

increased with increasing nitrogen oxidation ratio (NOR, which is defined as molar concentration of $NO_3^-/NO_3^-+NO_2$) as shown in Figure 6(c). Indeed, enhanced NOR, RH and ALWC were found under high $PM_{2.5}$ levels (see in Figure S4). All the findings suggested that hydrolysis of N_2O_5 contributed a major fraction to nitrate production under the high RH and high loadings of ALWC conditions in the haze events. However, the contribution of heterogeneous processes to nitrate formation decreased with increasing ozone concentration as shown in Figure 6(d). The hydrolysis of N_2O_5 contributed approximately 28 % to nitrate formation under higher ozone levels (O_3 > 40 μg m^{-3}), which was much lower than that (51 %) during low ozone level conditions (O_3 < 40 μg m^{-3}). This might reflect that heterogeneous reaction was not a major pathway of nitrate production during higher photochemical capacity. Instead, gas-phase oxidation was dominant formation pathway under high O_3 conditions. The formation mechanisms of nitrate aerosols were quantified, but uncertainty existed in the estimations. Continuous monitoring of some atmospheric oxidants (such as N_2O_5 and OH) are needed. They will provide valuable data for us to verify the reliability of nitrate formation mechanisms estimated by SIAR model.

3.4 Source apportionment of ambient NO_3^-

In this section, we attempted to use $\delta^{15}N\text{-}NO_3^-$ combined with SIAR model to quantify the potential sources of particulate nitrate in Beijing during the sampling period. According to previous studies, $\delta^{15}N$ values in particle NO_3^- would be much higher than that in atmospheric NO_x due to the fractionation process between NO_x and NO_3^- [*Chang et al.*, 2018; *Song et al.*, 2019]. Thus, the fractionation factors between $\delta^{15}N\text{-}NO_x$ and $\delta^{15}N\text{-}NO_3^-$ had to be considered when we quantified the nitrate sources using isotope techniques. The fractionation factors ($\varepsilon_{NO2\leftrightarrow NO3-}$) of NO_2 to NO_3^- can be estimated as [*Zong et al.*, 2017]:

$$\varepsilon_{NO2\leftrightarrow NO3-} = f_{N2O5} \times \varepsilon_{N2O5} + f_{OH} \times \varepsilon_{OH} \quad (12)$$

where f_{N2O5} and f_{OH} are the relative contributions of $N_2O_5 + H_2O$ and $NO_2 + OH$ to nitrate production as described in section.3.3. ε_{N2O5} and ε_{OH} are equilibrium isotope fractionation factors of NO_2 to NO_3^- through $N_2O_5 + H_2O$ and $NO_2 + OH\cdot$ reactions. Both values can be calculated as:

$$\varepsilon_{N2O5} = 1000 \times ({}^{15}\alpha_{N2O5/NO2} - 1) \quad (13)$$

$\varepsilon_{OH} = 1000 \times [(1 - f_{NO2}) ({}^{15}\alpha_{NO2/NO} - 1) / ((1 - f_{NO2}) + ({}^{15}\alpha_{NO2/NO} \times f_{NO2})]$ (14)

where f_{NO2} represents the ratio of NO_2 to NO_x in the atmosphere. ${}^{15}\alpha_{N2O5/NO2}$ (${}^{15}\alpha_{NO2/NO}$) is the equilibrium isotope fractionation factor in $\delta^{15}N$ between N_2O_5 and NO_2 (NO_2 and NO), and their values can be calculated by the following equations [*Walters and Michalski*, 2015]:

${}^{15}\alpha_{X/Y}\text{-}1 = A / T^4 \times 10^{10} + B / T^3 \times 10^8 + C / T^2 \times 10^6 + D / T \times 10^4$ (15)

where A, B, C and D are 0.69398, -1.9859, 2.3876 and -0.16308 for ${}^{15}\alpha_{N2O5/NO2}$. For ${}^{15}\alpha_{NO2/NO}$, A, B, C and D values are 3.8834, -7.7299, 6.0101 and -0.17928, respectively [*Walters and Michalski*, 2015]. Figure S5 shows the calculated fractionation factors of NO_2 to NO_3^- during the sampling period. The $\varepsilon_{NO2 \leftrightarrow NO3-}$ values fluctuated from 5.6 to 8.3 ‰ with an average value of 6.5 ‰.

According to the emission inventories by *Zhao et al.* [2012], coal combustion made a major contribution (~ 50 %) to total NO_x emissions in northern China; traffic and biomass burning contributed 31 % and 5 % to the total NO_x emissions, respectively. In addition, soil emission is also an important source of NO_x during the planting season of crops when NO_x is emitted as a by-product of nitrification and denitrification reactions in fertilized soils [*Felix and Elliott*, 2014; *Li and Wang*, 2008]. In the suburban Beijing, a large quantity of wheat is widely planted during both autumn and winter [*Ju et al*., 2003]. Therefore, soil emission was considered to quantify potential sources of nitrate in addition to coal combustion, traffic emissions and BB. In SIAR model, the $\delta^{15}N\text{-}NO_3^-$ in ambient aerosol samples and $\delta^{15}N\text{-}NO_x$ in emission sources served as input data to quantify potential sources of particulate nitrate. The $\delta^{15}N\text{-}NO_x$ values in various emission sources were obtained from the literatures, which were 1.0 ± 4.1 ‰ for biomass burning [*Hasting et al*., 2009; *Felix and Elliott*, 2013; *Fibiger and Hastings*, 2016], 13.7 ± 4.6 ‰ for coal combustion [*Felix et al.*, 2015; *Felix et al.*, 2012; *Walters et al.*, 2015a;], -3.2 ± 6.8 ‰ for vehicle emissions [*Walters et al.*, 2015b] and -33.77 ± 12.16 ‰ for soil emissions [*Felix and Elliott*, 2014; *Li and Wang*, 2008] (Table S1). As mentioned above, isotope fractionation occurs from NO_x converted to NO_3^-, the observed $\delta^{15}N\text{-}NO_3^-$ values needed to be corrected by subtracting the average calculated $\varepsilon_{NO2 \leftrightarrow NO3-}$ value (6.5 ‰, Figure S5). After correction, the observed $\delta^{15}N\text{-}NO_3^-$ should be ranged from -6.9 to 14.2 ‰ with a mean value of 4.9 ± 5.1 ‰. Finally, the corrected observed $\delta^{15}N\text{-}NO_3^-$ value in

each sample would serve as input data in SIAR model to estimate the source apportionments of particulate nitrate in Beijing.

Figure S6 shows the time series of the relative contribution of each source to particulate nitrate in Beijing during the sampling period. The average contributions of coal combustion, biomass burning, vehicle emission and soil emission to nitrate were 50, 26, 20 and 4 %, respectively. Our estimated contribution of coal combustion was in accordance with that of emission inventory of northern China while the contribution of traffic emissions was smaller than the emission inventory (~ 31%) [*Zhao et al.*, 2012]. Nevertheless, the contribution of BB was much higher than the emission inventory data [*Zhao et al.*, 2012], but similar to that (~27 %) in Beijing during the 2014 winter study [*Song et al*., 2019]. In northern China, BB activities frequently occurs due to burning crop residuals during the harvest seasons (spring and autumn) and residential heating as well as households in winter [*Cai et al.*, 2018]. Since the aerosol sampling was conducted in the autumn and winter, the significant contributions of BB to particulate nitrate were likely from the residential heating and household as well as the agriculture activities. Note that the $\delta^{15}N\text{-}NO_x$ values emitted by BB and vehicle exhausts overlapped, which might influence estimated source apportionments of BB and traffic emissions. In order to test the influences of the overlaps of $\delta^{15}N\text{-}NO_x$ on source uncertainties calculated by the SIAR model, we changed the original standard deviation of each emission source by -50 %, -30 %, -10 %, +10 %, +30 % and +50 %, respectively. Table S2 lists the source apportionments of nitrate aerosols when the standard deviation of $\delta^{15}N\text{-}NO_x$ in all emission sources were synchronously changed. For example, the original standard deviation of BB was 4.1 ‰ and we then changed the standard deviations to 2.05, 2.87, 3.69, 4.51, 5.33 and 6.15 ‰, respectively, for the test. The results showed that the contribution of each source to nitrate aerosols kept almost constant levels under different standard deviations, reflecting that the discrepancies of estimated source apportionments under the different standard deviations were very small and can be likely neglected. Also shown in Table S2, large standard deviation of relative contribution to nitrate in each emission source was found. However, when we estimated the source apportionment of nitrate by using individual sample, the standard deviation became quite small (Figure S6). This implied that the great uncertainty in terms of

source apportionments might be form the dispersed $\delta^{15}N\text{-}NO_3^-$ values (4.9 ± 5.1 ‰) in aerosol samples collected in Beijing.

In this work, the proportion of soil emission was only 4 %. To prove the necessity of this emission source serving as input to SIAR model, we made the comparison of the source apportionments of nitrate aerosols by three (scenario I) and four emission sources (scenario II). Figure S7 shows the SIAR output estimated in scenario I. Briefly, the contributions of coal combustion, biomass burning and vehicle emissions were 40, 30 and 30 %, respectively. Compared with the results of scenario II (Figure 8), coal combustion was still the most predominant source and the contribution of each source to nitrate in scenario I under different $PM_{2.5}$ levels was consistent with the results in scenario II. Moreover, the posterior distributions for the proportional contribution of scenario I and scenario II were compared (see in Figure S8). Although vehicle emissions and BB showed similar probability distributions in both scenarios, the correlation between vehicle emissions and BB in scenario II was much weakly negative than that of scenario I. This implied that no significant inter-influence between vehicle emissions and biomass burning in terms of estimated source apportionments when the four emission sources were considered in SIAR model [*Parnell et al*., 2010].

We further discussed the influences of air origins and transported routes on potential sources of particulate nitrate during the sampling period. As shown in Figure 7, a total of 83 backward trajectories were computed and all the air masses were categorized into three clusters. The air parcels of cluster 1 were mainly originated from southern areas of local Beijing. This air cluster accounted for 39 % of the total air masses. On the contrary, the air masses of cluster 2 came from Inner Mongolia, passing over northern Hebei Province and arriving at Beijing. The cluster 2 contributed 43 % to the total air parcels during the sampling period. The cluster 3 was originated from Hebei province and then transported to the receptor site. This air cluster accounted for 18 % of the total air masses. Interestingly, the discrepancies of NO_3^- concentration and its source apportionments among the three air clusters were also found. In cluster 1, the average NO_3^- concentration was 20.0 ± 18.4 μg m^{-3}, which exceeded the nitrate concentrations of cluster 2 (4.0 ± 10.7 μg m^{-3}) and cluster 3 (6.4 ± 6.8 μg m^{-3}) by factors of 5.0 and 3.1, respectively. On the other hand, the wind speed in cluster 1 (2.3 ± 0.8 m s^{-1}) were lower than that in cluster 2 (3.9 ± 1.4 m s^{-1}) and cluster 3 (2.8 ± 0.8 m s^{-1}). The lower wind

speed was favorable for the accumulation of air pollutants and resulted in high $PM_{2.5}$ (even nitrate) concentrations. In term of source apportionments of nitrate, in cluster 2, BB, coal combustion, vehicle exhausts and soil emission contributed 28, 49, 18 and 5 %, respectively, to NO_3^-. In cluster 3, the contributions of BB, coal combustion, vehicle exhausts and soil emission were 29, 51, 16 and 4 %, respectively. On the contrary, the contributions of biomass burning, coal combustion, vehicle emissions and soil emission to nitrate in Cluster 1 were 23, 46, 27 and 4 %, respectively. In 2017, the coal consumption in Beijing reduced approximately 10 million tons [*Dao et al*., 2019]. This might explain the lower contribution of coal burning in cluster 1 since the air parcels of this group were mainly from local Beijing where coal consumption has decreased in the past years. On the other hand, the relative contribution of traffic in cluster 1 was significantly higher than those of cluster 2 and 3, suggesting enhanced local traffic contribution to nitrate aerosols in Beijing.

In addition, we also explored the potential sources of nitrate aerosols during the different air quality conditions. During the clean period, the contributions of BB, coal combustion, vehicle exhausts and soil emission to nitrate were 26, 51, 18 and 5 %, respectively (see in Figure 8). When severe haze pollution occurred, the contributions of BB, coal combustion, vehicle exhausts and soil emission to nitrate were 29, 31, 30 and 10 %, respectively. Our results did elucidate that enhancement of the contribution of vehicle exhausts to particulate NO_3^- were found in Beijing under severe polluted conditions. Previously, residential heating with coal combustion was a major source to induce the haze formation in Beijing [*Cai et al.*, 2018]. Nevertheless, the coal combustion for residential heating has been replaced by burning of natural gas in recent years. This might explain that the relative suppressed contribution of coal burning to nitrate aerosols during the haze events.

In this work, we used the Monte Carlo approach in SIAR model to quantify the formation mechanisms and source apportionments of ambient nitrate aerosols. Although SIAR model can produce precise estimates, some uncertainty still existed in this statistical model. Thus, certain measures suggested here may reduce the model uncertainty and improve the model accuracy. First, the ambient samples served as input should have the same natural attributes. This could eliminate the uncertainty caused by the different attributes between input data, such as the great differences of $\delta^{15}N\text{-}NO_3^-$ values between the wintertime and summertime samples. Second,

SIAR model is very sensitive to missing sources; causes biases on the proportion estimates for other sources if all sources are not included. The discriminatory power of mixing model generally declines with the number of sources [*Phillips et al*., 2014]. Thus, inclusion of all potential sources served as input in an informed way are needed. On the other hand, the isotope compositions of emission sources exhibit territorial distributions. This suggested that establishments of isotope compositions in local emissions may be another way to reduce the model uncertainty. Isotope compositions among various sources are required to be the greatest extents, and the isotope values of samples should be within the borders of all emission sources. The posterior distributions of output (e.g. the probability distribution of each source and the correlations between all emission sources) in SIAR model should be reported. This provide the valuable information to inspect the inter-influence between any two emission sources resolved by SIAR model [*Parnell et al*., 2010].

4. Conclusions and implications

In this study, we explored the formation mechanisms and source apportionments of nitrate in $PM_{2.5}$ in Beijing during November 13 to December 24, 2018 through the isotope techniques. The results indicated that heterogeneous reaction constituted a major fraction (64 %) of nitrate production during the haze period, which was 1.6 time higher than that (39 %) during the clean period. Coal combustion, biomass burning and traffic emissions were major sources of nitrate, contributing 50, 26 and 20 % to particulate nitrate, respectively, during the sampling period. Most importantly, significant enhanced contribution of vehicle emissions from 18 % during the clear period to 30 % during the haze period were found, indicating that traffic emissions were the major contributing sources to nitrate when poor air quality was observed in Beijing.

In northern China, haze pollution frequently occurs in both autumntime and wintertime to deteriorate the air quality and threaten the human health. Previously, coal combustion constituted to a major fraction (~ 50 %) of ambient NO_x in northern China [*Zhao et al.*, 2012] and was also a dominant source induced wintertime haze formation. Since 2013, the Beijing Gas Group began cutting down the consumption of coal usage for residential heating; instead, natural gas was used to be substantial energy. This measure decreased not only sulfate concentrations, but also nitrate levels since coal burning was a main source of NO_x [*Zhao et*

al., 2012]. Before the clean air actions, the contribution of coal combustion to nitrate aerosols in Beijing during the wintertime was 71 % [*Luo et al*., 2019]. Nevertheless, the contribution dropped to 50 % in 2018 (this work), suggesting that contribution of coal combustion to nitrate has significant decreased via clean air actions.

Although the existence of uncertainty was found in SIAR model, it is still a useful tool to quantify potential sources of atmospheric particulate with isotope techniques. Utilization of SIAR model results, the evolutions in contributions of various sources to nitrate in Beijing were discussed by comparing with the earlier studies. Moreover, enhancements of traffic emissions contributed to nitrate were found. This implied that control traffic emissions might be a good way to decrease nitrate concentrations in the future.

5. Acknowledgements

This study was financially supported by the National Key R&D Program of China (Grant No. 2017YFC0212704), the Natural Scientific Foundation of China (No. 91644103 and 41603104) and the Provincial Natural Science Foundation of Jiangsu (Grant No. BK20180040). All the data used in this paper are available from the Open Science Framework (https://osf.io/6kq2a).

References

Alexander, B., M. G. Hastings, D. J. Allman, J. Dachs, J. A. Thornton, and S. A. Kunasek (2009), Quantifying atmospheric nitrate formation pathways based on a global model of the oxygen isotopic composition ($\Delta^{17}O$) of atmospheric nitrate, *Atmos. Chem. Phys.*, *9*(14), 5043-5056, doi:10.5194/acp-9-5043-2009.

Bäumer, D., B. Vogel, S. Versick, R. Rinke, O. Möhler, and M. Schnaiter (2008), Relationship of visibility, aerosol optical thickness and aerosol size distribution in an ageing air mass over South-West Germany, *Atmospheric Environment*, *42*(5), 989-998, doi:https://doi.org/10.1016/j.atmosenv.2007.10.017.

Böhlke, J. K., S. J. Mroczkowski, and T. B. Coplen (2003), Oxygen isotopes in nitrate: new reference materials for ^{18}O:^{17}O:^{16}O measurements and observations on nitrate-water equilibration, *Rapid Communications in Mass Spectrometry*, *17*(16), 1835-1846, doi:10.1002/rcm.1123.

Cai, S., Q. Li, S. Wang, J. Chen, D. Ding, B. Zhao, D. Yang, and J. Hao (2018), Pollutant emissions from residential combustion and reduction strategies estimated via a village-based emission inventory in Beijing, *Environmental Pollution*, *238*, 230-237, doi:https://doi.org/10.1016/j.envpol.2018.03.036.

Chang, Y., Y. Zhang, C. Tian, S. Zhang, X. Ma, F. Cao, X. Liu, W. Zhang, T. Kuhn, and M. F. Lehmann (2018), Nitrogen isotope fractionation during gas-to-particle conversion of NO_x to NO_3^- in the atmosphere - implications for isotope-based NO_x source apportionment, *Atmos. Chem. Phys.*, *18*(16), 11647-11661, doi:10.5194/acp-18-11647-2018.

Clark, C. M., and D. Tilman (2008), Loss of plant species after chronic low-level nitrogen deposition to prairie grasslands, *Nature*, *451*, 712, doi:10.1038/nature06503https://www.nature.com/articles/nature06503#supplementary-information.

Dao, X., Y.-C. Lin, F. Cao, S.-Y. Di, Y. Hong, G. Xing, J. Li, P. Fu, and Y.-L. Zhang (2019), Introduction to the Aerosol Chemical Composition Monitoring Network of China: Objectives, Current Status and Outlook, Bulletin of the American Meteorological Society, doi:10.1175/BAMS-D-18-0325.1.

Deng, H., H. Tan, F. Li, M. Cai, P. W. Chan, H. Xu, X. Huang, and D. Wu (2016), Impact of

relative humidity on visibility degradation during a haze event: A case study, *Science of The Total Environment*, *569-570*, 1149-1158, doi:https://doi.org/10.1016/j.scitotenv.2016.06.190.

Draxler, R. R., and G. Hess (1998), An overview of the HYSPLIT_4 modelling system for trajectories, *Australian meteorological magazine*, *47*(4), 295-308.

Du, C., S. Liu, X. Yu, X. Li, C. Chen, Y. Peng, Y. Dong, Z. Dong, and F. Wang (2013), Urban boundary layer height characteristics and relationship with particulate matter mass concentrations in Xi'an, central China.

Dubey, M. K., R. Mohrschladt, N. M. Donahue, and J. G. Anderson (1997), Isotope specific kinetics of hydroxyl radical (OH) with water (H2O): Testing models of reactivity and atmospheric fractionation, The Journal of Physical Chemistry A, 101(8), 1494-1500.

Elliott, E. M., C. Kendall, S. D. Wankel, D. A. Burns, E. W. Boyer, K. Harlin, D. J. Bain, and T. J. Butler (2007), Nitrogen Isotopes as Indicators of NO_x Source Contributions to Atmospheric Nitrate Deposition Across the Midwestern and Northeastern United States, *Environmental Science & Technology*, *41*(22), 7661-7667, doi:10.1021/es070898t.

Fan, M.-Y., et al. (2019), Isotope-based source apportionment of nitrogen-containing aerosols: A case study in an industrial city in China, *Atmospheric Environment*, *212*, 96-105, doi:https://doi.org/10.1016/j.atmosenv.2019.05.020.

Felix, J. D., and E. M. Elliott (2014), Isotopic composition of passively collected nitrogen dioxide emissions: Vehicle, soil and livestock source signatures, *Atmospheric Environment*, *92*, 359-366, doi:https://doi.org/10.1016/j.atmosenv.2014.04.005.

Felix, J. D., E. M. Elliott (2013), The agricultural history of human-nitrogen interactions as recorded in ice core $\delta^{15}N\text{-}NO_3^-$, *Geophy. Res. Lett., 40*, (8), 1642-1646.

Felix, J. D., E. M. Elliott, and S. L. Shaw (2012), Nitrogen Isotopic Composition of Coal-Fired Power Plant NO_x: Influence of Emission Controls and Implications for Global Emission Inventories, *Environmental Science & Technology*, *46*(6), 3528-3535, doi:10.1021/es203355v.

Felix, J. D., E. M. Elliott, G. B. Avery, R. J. Kieber, R. N. Mead, J. D. Willey, and K. M. Mullaugh (2015), Isotopic composition of nitrate in sequential Hurricane Irene precipitation samples: Implications for changing NO_x sources, *Atmospheric Environment*,

106, 191-195, doi:https://doi.org/10.1016/j.atmosenv.2015.01.075.

Fibiger, D. L., and M. G. Hastings (2016), First Measurements of the Nitrogen Isotopic Composition of NO_x from Biomass Burning, *Environmental Science & Technology*, *50*(21), 11569-11574, doi:10.1021/acs.est.6b03510.

Fountoukis, C., A. Nenes (2007) ISORROPIA II: a computationally efficient thermodynamic equilibrium model for K^+–Ca^{2+}–Mg^{2+}–NH_4^+–Na^+–SO_4^{2-}–NO_3^-–Cl^-–H_2O aerosols. *Atmos. Chem. Phys*., 7 (17), pp. 4639-4659.

Freyer, H. D. (1991), Seasonal variation of $^{15}N/^{14}N$ ratios in atmospheric nitrate species, *Tellus B*, *43*(1), 30-44, doi:10.1034/j.1600-0889.1991.00003.x.

Hastings, M. G., D. M. Sigman, and F. Lipschultz (2003), Isotopic evidence for source changes of nitrate in rain at Bermuda, *Journal of Geophysical Research: Atmospheres*, *108*(D24).

Hastings, M. G., J. C. Jarvis, and E. J. Steig (2009), Anthropogenic impacts on nitrogen isotopes of ice-core nitrate. *Science, 324*, (5932), 1288-1288.

He, P., Z. Xie, X. Yu, L. Wang, H. Kang, and F. Yue (2020), The observation of isotopic compositions of atmospheric nitrate in Shanghai China and its implication for reactive nitrogen chemistry, *Science of The Total Environment*, *714*, 136727, doi:https://doi.org/10.1016/j.scitotenv.2020.136727.

Huang, R.-J., et al. (2014), High secondary aerosol contribution to particulate pollution during haze events in China, *Nature*, *514*, 218, doi:10.1038/nature13774 https://www.nature.com/articles/nature13774#supplementary-information.

Huang, X.-F., M. Hu, L.-Y. He, and X.-Y. Tang (2005), Chemical characterization of water-soluble organic acids in $PM_{2.5}$ in Beijing, China, Atmospheric Environment, 39(16), 2819-2827, doi:https://doi.org/10.1016/j.atmosenv.2004.08.038.

Johnston, J. C., and M. H. Thiemens (1997), The isotopic composition of tropospheric ozone in three environments, Journal of Geophysical Research: Atmospheres, 102(D21), 25395-25404.

Ju, X.-t., J.-r. Pan, X.-j. Liu, and F.-s. Zhang (2003), Study on the fate of nitrogen fertilizer in winter wheat/summer maize rotation system in Beijing suburban, Plant Nutrition and Fertilizing Science, 3.

Kamezaki, K., S. Hattori, Y. Iwamoto, S. Ishino, H. Furutani, Y. Miki, M. Uematsu, K. Miura,

and N. Yoshida (2019), Tracing the sources and formation pathways of atmospheric particulate nitrate over the Pacific Ocean using stable isotopes, *Atmospheric Environment*, *209*, 152-166, doi:https://doi.org/10.1016/j.atmosenv.2019.04.026.

Kendall, C., E. M. Elliott, and S. D. Wankel (2007), Tracing Anthropogenic Inputs of Nitrogen to Ecosystems, *Stable Isotopes in Ecology and Environmental Science*, doi: 10.1002/9780470691854.ch1210.1002/9780470691854.ch12.

Khoder, M. (2002), Atmospheric conversion of sulfur dioxide to particulate sulfate and nitrogen dioxide to particulate nitrate and gaseous nitric acid in an urban area, Chemosphere, 49(6), 675-684.

Li, D., and X. Wang (2008), Nitrogen isotopic signature of soil-released nitric oxide (NO) after fertilizer application, *Atmospheric Environment*, *42*(19), 4747-4754, doi:https://doi.org/10.1016/j.atmosenv.2008.01.042.

Li, H., Q. Zhang, B. Zheng, C. Chen, N. Wu, H. Guo, Y. Zhang, Y. Zheng, X. Li, and K. He (2018), Nitrate-driven urban haze pollution during summertime over the North China Plain, *Atmos. Chem. Phys.*, *18*(8), 5293-5306, doi:10.5194/acp-18-5293-2018.

Liu, J., et al. (2014), Source Apportionment Using Radiocarbon and Organic Tracers for $PM_{2.5}$ Carbonaceous Aerosols in Guangzhou, South China: Contrasting Local- and Regional-Scale Haze Events, *Environmental Science & Technology*, *48*(20), 12002-12011, doi:10.1021/es503102w.

Luo, L., Y. Wu, H. Xiao, R. Zhang, H. Lin, X. Zhang, and S.-j. Kao (2019), Origins of aerosol nitrate in Beijing during late winter through spring, *Science of The Total Environment*, *653*, 776-782, doi:https://doi.org/10.1016/j.scitotenv.2018.10.306.

Morin, S., J. Savarino, M. M. Frey, N. Yan, S. Bekki, J. W. Bottenheim, and J. M. F. Martins (2008), Tracing the Origin and Fate of NO_x in the Arctic Atmosphere Using Stable Isotopes in Nitrate, *Science*, *322*(5902), 730, doi:10.1126/science.1161910.

Pan, Y., et al. (2016), Redefining the importance of nitrate during haze pollution to help optimize an emission control strategy, *Atmospheric Environment*, *141*, 197-202, doi:https://doi.org/10.1016/j.atmosenv.2016.06.035.

Park, Y.-m., et al. (2018), Characterizing isotopic compositions of TC-C, $NO3^-$-N, and NH_4^+-N in $PM_{2.5}$ in South Korea: Impact of China's winter heating, *Environmental Pollution*, *233*,

735-744, doi:https://doi.org/10.1016/j.envpol.2017.10.072.

Parnell, A. C., R. Inger, S. Bearhop, and A. L. Jackson (2010), Source Partitioning Using Stable Isotopes: Coping with Too Much Variation, *PLOS ONE*, *5*(3), e9672, doi:10.1371/journal.pone.0009672.

Phillips, D. L., R. Inger, S. Bearhop, A. L. Jackson, J. W. Moore, A. C. Parnell, B. X. Semmens, and E. J. Ward (2014), Best practices for use of stable isotope mixing models in food-web studies, Canadian Journal of Zoology, 92(10), 823-835.

Savarino, J., J. Kaiser, S. Morin, D. M. Sigman, and M. H. Thiemens (2007), Nitrogen and oxygen isotopic constraints on the origin of atmospheric nitrate in coastal Antarctica, *Atmos. Chem. Phys.*, *7*(8), 1925-1945, doi:10.5194/acp-7-1925-2007.

Song, W., Y.-L. Wang, W. Yang, X.-C. Sun, Y.-D. Tong, X.-M. Wang, C.-Q. Liu, Z.-P. Bai, and X.-Y. Liu (2019), Isotopic evaluation on relative contributions of major NO_x sources to nitrate of $PM_{2.5}$ in Beijing, *Environmental Pollution*, *248*, 183-190, doi:https://doi.org/10.1016/j.envpol.2019.01.081.

Sun, P., Nie, W., Chi, X., Xie, Y., Huang, X., Xu, Z., Qi, X., Xu, Z., Wang, L., Wang, T., Zhang, Q., and Ding, A (2018), Two years of online measurement of fine particulate nitrate in the western Yangtze River Delta: influences of thermodynamics and N_2O_5 hydrolysis, *Atmos. Chem. Phys.*, *18*(23), 17177-17190, doi:10.5194/acp-18-17177-2018.

Tan, H., M. Cai, Q. Fan, L. Liu, F. Li, P. W. Chan, X. Deng, and D. Wu (2017), An analysis of aerosol liquid water content and related impact factors in Pearl River Delta, *Science of The Total Environment*, *579*, 1822-1830, doi:https://doi.org/10.1016/j.scitotenv.2016.11.167.

Vicars, W. C., et al. (2013), Spatial and diurnal variability in reactive nitrogen oxide chemistry as reflected in the isotopic composition of atmospheric nitrate: Results from the CalNex 2010 field study, *Journal of Geophysical Research: Atmospheres*, *118*(18), 10,567-510,588, doi:10.1002/jgrd.50680.

Walters, W. W., and G. Michalski (2015), Theoretical calculation of nitrogen isotope equilibrium exchange fractionation factors for various NO_y molecules, *Geochimica et Cosmochimica Acta*, *164*, 284-297, doi:https://doi.org/10.1016/j.gca.2015.05.029.

Walters, W. W., and G. Michalski (2016), Theoretical calculation of oxygen equilibrium isotope fractionation factors involving various NO_y molecules, OH, and H_2O and its implications

for isotope variations in atmospheric nitrate, *Geochimica et Cosmochimica Acta*, *191*, 89-101, doi:https://doi.org/10.1016/j.gca.2016.06.039.

Walters, W. W., B. D. Tharp, H. Fang, B. J. Kozak, and G. Michalski (2015a), Nitrogen Isotope Composition of Thermally Produced NO_x from Various Fossil-Fuel Combustion Sources, *Environmental Science & Technology*, *49*(19), 11363-11371, doi:10.1021/acs.est.5b02769.

Walters, W. W., D. S. Simonini, and G. Michalski (2016), Nitrogen isotope exchange between NO and NO_2 and its implications for $\delta^{15}N$ variations in tropospheric NO_x and atmospheric nitrate, *Geophysical Research Letters*, *43*(1), 440-448, doi:10.1002/2015GL066438.

Walters, W. W., S. R. Goodwin, and G. Michalski (2015b), Nitrogen Stable Isotope Composition ($\delta^{15}N$) of Vehicle-Emitted NO_x, *Environmental Science & Technology*, *49*(4), 2278-2285, doi:10.1021/es505580v.

Wang, H., et al. (2017), High N_2O_5 Concentrations Observed in Urban Beijing: Implications of a Large Nitrate Formation Pathway, *Environmental Science & Technology Letters*, *4*(10), 416-420, doi:10.1021/acs.estlett.7b00341.

Wang, H., K. Lu, X. Chen, Q. Zhu, Z. Wu, Y. Wu, and K. Sun (2018), Fast particulate nitrate formation via N_2O_5 uptake aloft in winter in Beijing, Atmospheric Chemistry and Physics, 18(14), 10483-10495.

Wang, Y.-L., W. Song, W. Yang, X.-C. Sun, Y.-D. Tong, X.-M. Wang, C.-Q. Liu, Z.-P. Bai, and X.-Y. Liu (2019), Influences of Atmospheric Pollution on the Contributions of Major Oxidation Pathways to $PM_{2.5}$ Nitrate Formation in Beijing, *Journal of Geophysical Research: Atmospheres*, *124*(7), 4174-4185, doi:10.1029/2019JD030284.

Wankel, S. D., Y. Chen, C. Kendall, A. F. Post, and A. Paytan (2010), Sources of aerosol nitrate to the Gulf of Aqaba: Evidence from $\delta^{15}N$ and $\delta^{18}O$ of nitrate and trace metal chemistry, *Marine Chemistry*, *120*(1-4), 90-99.

Yan, C., Y. J. Tham, Q. Zha, X. Wang, L. Xue, J. Dai, Z. Wang, and T. Wang (2019), Fast heterogeneous loss of N_2O_5 leads to significant nighttime NO_x removal and nitrate aerosol formation at a coastal background environment of southern China, Science of The Total Environment, 677, 637-647, doi:https://doi.org/10.1016/j.scitotenv.2019.04.389.

Yu, Q., J. Chen, W. Qin, S. Cheng, Y. Zhang, M. Ahmad, and W. Ouyang (2019), Characteristics and secondary formation of water-soluble organic acids in PM_1, $PM_{2.5}$ and PM_{10} in Beijing

during haze episodes, *Science of The Total Environment*, *669*, 175-184, doi:https://doi.org/10.1016/j.scitotenv.2019.03.131.

Zhang, F., Z.-w. Wang, H.-r. Cheng, X.-p. Lv, W. Gong, X.-m. Wang, and G. Zhang (2015), Seasonal variations and chemical characteristics of $PM_{2.5}$ in Wuhan, central China, *Science of The Total Environment*, *518-519*, 97-105, doi:https://doi.org/10.1016/j.scitotenv.2015.02.054.

Zhang, Q., et al. (2017), Transboundary health impacts of transported global air pollution and international trade, *Nature*, *543*, 705, doi:10.1038/nature21712https://www.nature.com/articles/nature21712#supplementary-information.

Zhang, T., et al. (2011), Water-soluble ions in atmospheric aerosols measured in Xi'an, China: Seasonal variations and sources, *Atmospheric Research*, *102*(1), 110-119, doi:https://doi.org/10.1016/j.atmosres.2011.06.014.

Zhang, X., X. Zhao, G. Ji, R. Ying, Y. Shan, and Y. Lin (2019), Seasonal variations and source apportionment of water-soluble inorganic ions in $PM_{2.5}$ in Nanjing, a megacity in southeastern China, *Journal of Atmospheric Chemistry*, *76*(1), 73-88, doi:10.1007/s10874-019-09388-z.

Zhang, Y., Y. Jia, M. Li, and L. a. Hou (2018), The characterization of water-soluble inorganic ions in $PM_{2.5}$ during a winter period in Xi'an, China, *Environmental Forensics*, *19*(3), 166-171, doi:10.1080/15275922.2018.1474975.

Zhao, B., P. Wang, J. Z. Ma, S. Zhu, A. Pozzer, and W. Li (2012), A high-resolution emission inventory of primary pollutants for the Huabei region, China, *Atmos. Chem. Phys.*, *12*(1), 481-501, doi:10.5194/acp-12-481-2012.

Zhao, Z.-Y., F. Cao, W.-Q. Zhang, X.-Y. Zhai, Y. Fang, M.-Y. Fan, and Y.-L. Zhang (2019), Determination of Stable Nitrogen and Oxygen Isotope Ratios in Atmospheric Aerosol Nitrates, *Chinese Journal of Analytical Chemistry*, *47*(6), 907-915, doi:https://doi.org/10.1016/S1872-2040(19)61166-7.

Zheng, B., et al. (2018), Trends in China's anthropogenic emissions since 2010 as the consequence of clean air actions, *Atmos. Chem. Phys.*, *18*(19), 14095-14111, doi:10.5194/acp-18-14095-2018.

Zong, Z., X. Wang, C. Tian, Y. Chen, Y. Fang, F. Zhang, C. Li, J. Sun, J. Li, and G. Zhang (2017), First Assessment of NO_x Sources at a Regional Background Site in North China Using Isotopic Analysis Linked with Modeling, *Environmental Science & Technology*, *51*(11), 5923-5931, doi:10.1021/acs.est.6b06316.

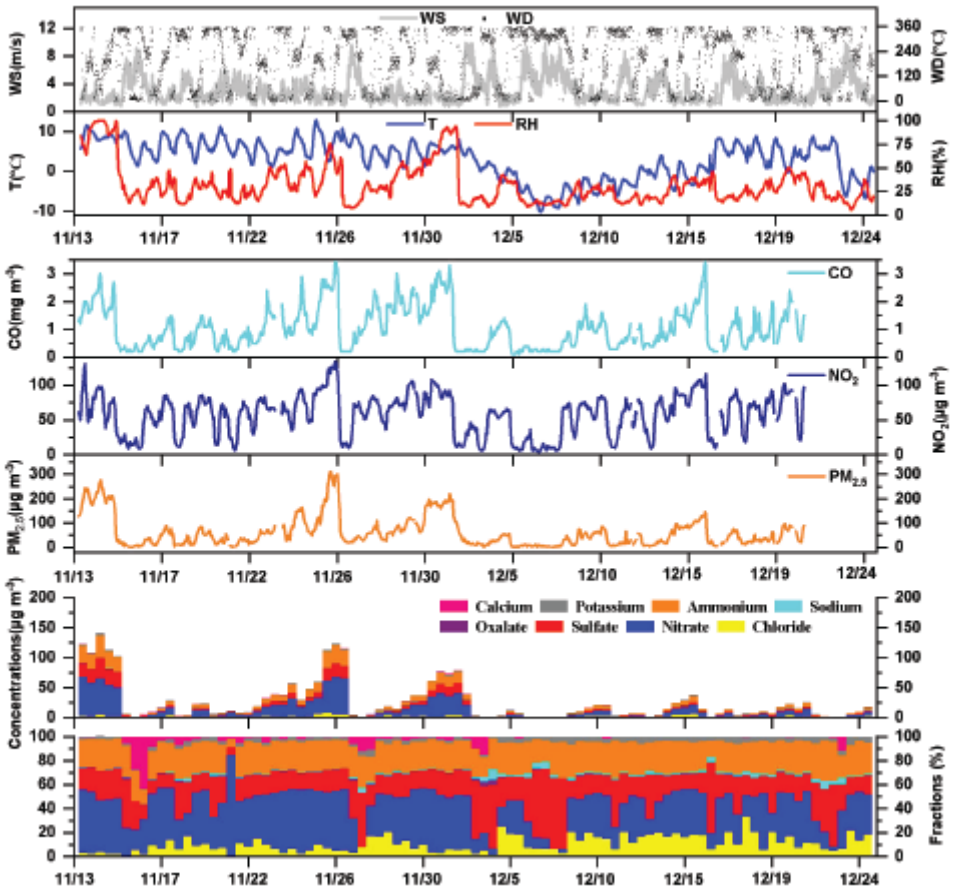

Figure 1 Time series of meteorological parameters, trace gases, ions and $PM_{2.5}$ in Beijing during the sampling period.

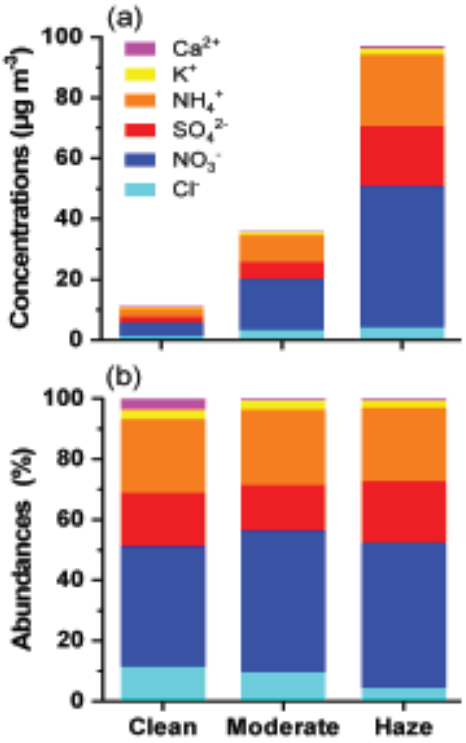

Figure 2 (a) Concentrations of ions and (b) their relative abundances to $PM_{2.5}$ mass in Beijing under different pollution levels.

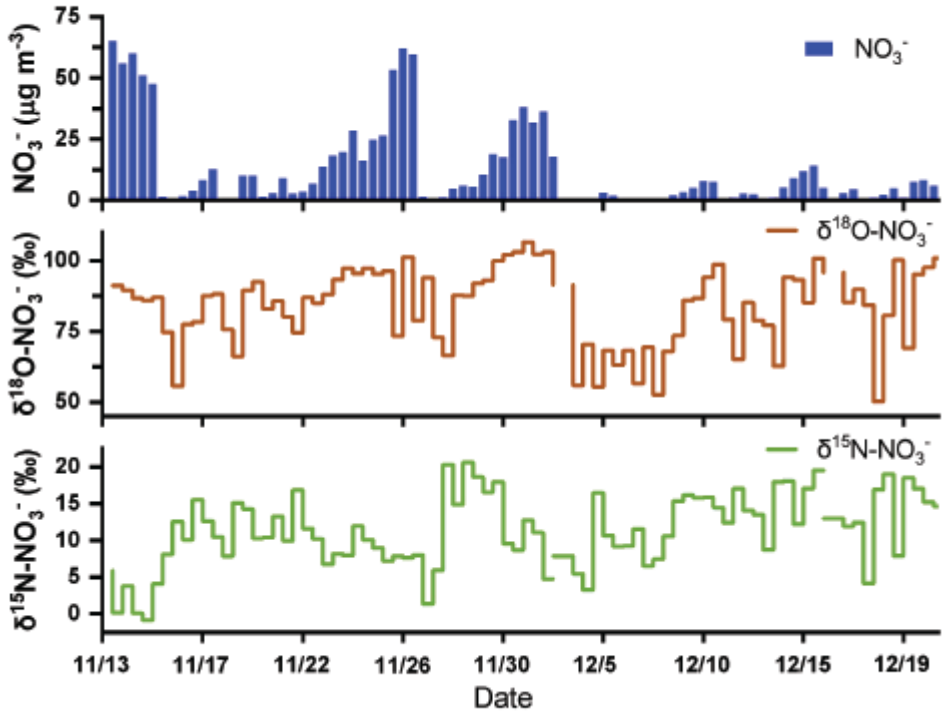

Figure 3 Time series of nitrate concentrations, $\delta^{15}N\text{-}NO_3^-$ and $\delta^{18}O\text{-}NO_3^-$ in Beijing during the sampling period.

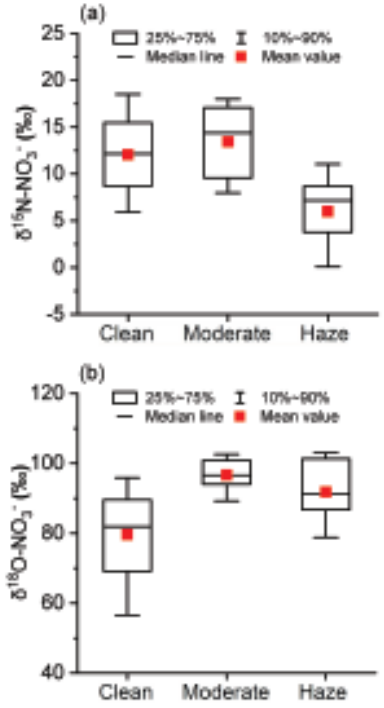

Figure 4 (a) δ^{15}N-NO_3^- and (b) δ^{18}O-NO_3^- values in $PM_{2.5}$ in Beijing under different polluted levels.

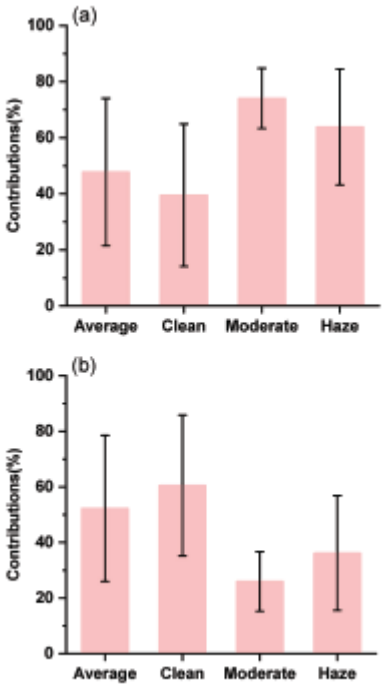

Figure 5 The relative contributions of (a) N_2O_5 and (b) $OH\cdot$ pathways of nitrate formation under different pollution levels.

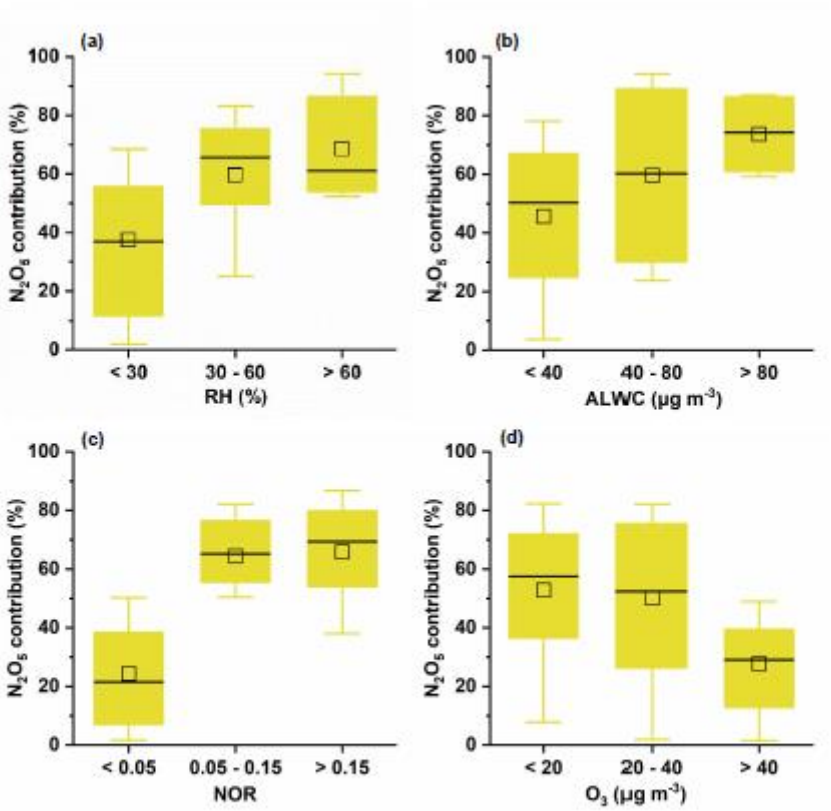

Figure 6 Contributions of N_2O_5 pathway under different levels of (a) relative humidity (RH), (b) ALWC, (c) NOR and (d) O_3.

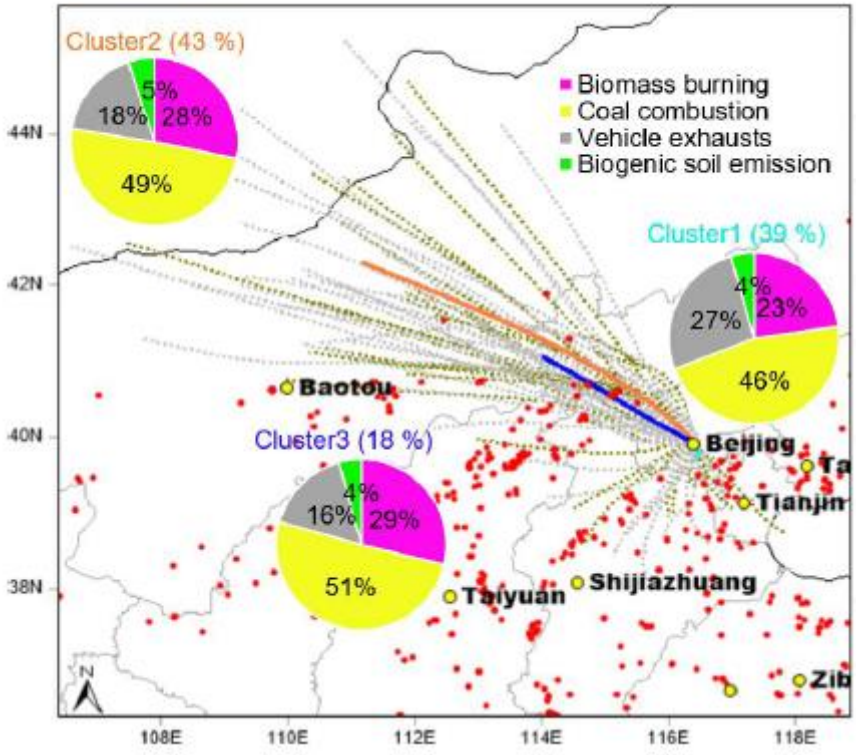

Figure 7 Source apportionments of $PM_{2.5}$ nitrate in Beijing in the different air clusters (Brown yellow dotted lines represent the daytime trajectories; Grey dotted lines represent the nighttime trajectories).

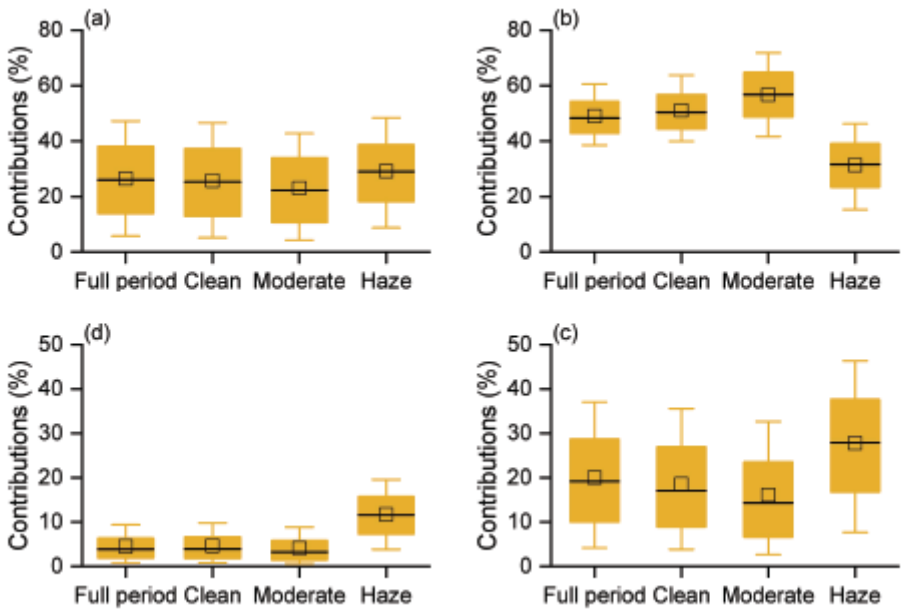

Figure 8 The relative contributions of (a) biomass burning, (b) coal combustion, (c) vehicle exhausts and (d) soil emission to $PM_{2.5}$ NO_3^- in Beijing under different air quality conditions. The whiskers and line in each box meant 10^{th} – 90^{th} percentiles and mean value, and the box encompassed the 25^{th} – 75^{th} percentiles, respectively.

Table 1 Average concentrations of $PM_{2.5}$ mass, ionic species, and gaseous pollutants along with meteorological parameters observed in Beijing during the sampling period.

Species	Average	Daytime	Nighttime	Clean	Moderate	Haze
N	83	41	42	60	10	13
$PM_{2.5}$ (μg m^{-3})	69.3 ± 68.9	65.2 ± 73.5	73.4 ± 64.6	34.0 ± 20.7	100.4 ± 19.9	208.5 ± 45.2
TWSIIs (μg m^{-3})	26.7 ± 34.6	27.0 ± 38.5	26.5 ± 30.5	11.4 ± 10.2	37.1 ± 17.5	100.2 ± 29.9
NO_3^- (μg m^{-3})	11.8 ± 16.7	12.2 ± 18.3	11.5 ± 15.1	4.4 ± 4.7	16.8 ± 9.7	46.6 ± 15.0
SO_4^{2-} (μg m^{-3})	4.8 ± 6.9	5.0 ± 7.7	4.7 ± 5.9	1.9 ± 1.5	5.4 ± 2.7	19.7 ± 7.0
NH_4^+ (μg m^{-3})	6.4 ± 8.2	6.5 ± 9.3	6.3 ± 7.0	2.7 ± 2.4	9.0 ± 4.0	23.7 ± 7.3
Cl^- (μg m^{-3})	1.9 ± 1.8	1.6 ± 1.8	2.3 ± 1.7	1.3 ± 1.2	3.5 ± 1.8	4.3 ± 1.8
Ca^{2+} (μg m^{-3})	0.4 ± 0.5	0.4 ± 0.6	0.4 ± 0.5	0.4 ± 0.5	0.2 ± 0.1	0.7 ± 0.6
K^+ (μg m^{-3})	0.7 ± 0.7	0.6 ± 0.8	0.7 ± 0.6	0.3 ± 0.3	1.1 ± 0.4	2.0 ± 0.6
Na^+ (μg m^{-3})	0.2 ± 0.1	0.1 ± 0.1	0.2 ± 0.1	0.1 ± 0.1	0.2 ± 0.1	0.3 ± 0.1
$C_2O_4^{2-}$ (μg m^{-3})	0.2 ± 0.2	0.2 ± 0.3	0.1 ± 0.2	0.1 ± 0.0	0.2 ± 0.1	0.5 ± 0.3
TWSIIs/$PM_{2.5}$	0.4 ± 0.2	0.4 ± 0.2	0.3 ± 0.1	0.3 ± 0.2	0.3 ± 0.1	0.5 ± 0.1
NO_3^-/SO_4^{2-}	1.9 ± 1.1	1.9 ± 1.1	1.9 ± 1.1	1.9 ± 1.8	3.1 ± 0.4	2.4 ± 0.4
SO_2 (μg m^{-3})	8.6 ± 5.6	8.3 ± 5.7	9.0 ± 5.5	8.0 ± 5.4	13.1 ± 5.4	8.0 ± 5.3
NO_2 (μg m^{-3})	58.9 ± 27.8	51.3 ± 28.7	66.7 ± 24.8	48.4 ± 22.5	80.3 ± 20.0	90.8 ± 21.2
CO (mg m^{-3})	1.1 ± 0.7	1.0 ± 0.7	1.2 ± 0.7	0.8 ± 0.4	1.6 ± 0.5	2.3 ± 0.5
O_3 (μg m^{-3})	21.0 ± 18.4	28.5 ± 17.9	13.3 ± 15.7	24.3 ± 19.7	12.2 ± 14.2	12.5 ± 8.7
RH (%)	33.0 ± 20.8	31.3 ± 22.5	34.8 ± 19.1	24.8 ± 9.3	39.2 ± 12.6	74.5 ± 18.3
Temperature (ºC)	3.3 ± 4.6	4.0 ± 4.6	2.7 ± 4.4	2.7 ± 4.7	4.1 ± 3.6	7.2 ± 1.8
WS (m/s)	3.1 ± 1.4	3.2 ± 1.4	3.0 ± 1.5	3.3 ± 1.3	2.5 ± 1.8	2.2 ± 1.1
ALWC (μg m^{-3})	12.6 ± 36.1	13.0 ± 40.6	12.2 ± 31.6	1.6 ± 2.3	10.7 ± 8.6	89.8 ± 70.5
$\delta^{15}N$-NO_3^- (‰)	11.5 ± 5.0	12.4 ± 5.1	10.4 ± 4.7	12.0 ± 4.5	13.4 ± 4.3	6.0 ± 4.2
$\delta^{18}O$-NO_3^- (‰)	83.8 ± 13.4	85.6 ± 10.2	81.1 ± 16.6	79.6 ± 13.3	96.7 ± 5.3	91.8 ± 9.8